ECONSTOR
Make Your Publications Visible.

A Service of

ZBW Leibniz-Informationszentrum Wirtschaft
Leibniz Information Centre for Economics

El Mourabit, Youness et al.

Article

Implementation and validation of backstepping control for PMSG wind turbine using dSPACE controller board

Energy Reports

Provided in Cooperation with:
Elsevier

Suggested Citation: El Mourabit, Youness et al. (2019) : Implementation and validation of backstepping control for PMSG wind turbine using dSPACE controller board, Energy Reports, ISSN 2352-4847, Elsevier, Amsterdam, Vol. 5, pp. 807-821, https://doi.org/10.1016/j.egyr.2019.06.015

This Version is available at:
https://hdl.handle.net/10419/243629

Standard-Nutzungsbedingungen:

Die Dokumente auf EconStor dürfen zu eigenen wissenschaftlichen Zwecken und zum Privatgebrauch gespeichert und kopiert werden.

Sie dürfen die Dokumente nicht für öffentliche oder kommerzielle Zwecke vervielfältigen, öffentlich ausstellen, öffentlich zugänglich machen, vertreiben oder anderweitig nutzen.

Sofern die Verfasser die Dokumente unter Open-Content-Lizenzen (insbesondere CC-Lizenzen) zur Verfügung gestellt haben sollten, gelten abweichend von diesen Nutzungsbedingungen die in der dort genannten Lizenz gewährten Nutzungsrechte.

Terms of use:

Documents in EconStor may be saved and copied for your personal and scholarly purposes.

You are not to copy documents for public or commercial purposes, to exhibit the documents publicly, to make them publicly available on the internet, or to distribute or otherwise use the documents in public.

If the documents have been made available under an Open Content Licence (especially Creative Commons Licences), you may exercise further usage rights as specified in the indicated licence.


https://creativecommons.org/licenses/by-nc-nd/4.0/

WWW.ECONSTOR.EU

Mitglied der Leibniz-Gemeinschaft

Energy Reports 5 (2019) 807–821

Contents lists available at ScienceDirect

Energy Reports

journal homepage: www.elsevier.com/locate/egyr

Research paper

Implementation and validation of backstepping control for PMSG wind turbine using dSPACE controller board

El Mourabit Youness [a,*], Derouich Aziz [a], El Ghzizal Abdelaziz [a], Bouchnaif Jamal [b], El Ouanjli Najib [a], Zamzoum Othmane [a], Mezioui Khalid [b], Badre BOSSOUFI [b]

[a] Laboratory of Production Engineering, Energy and Sustainable Development, Higher School of Technology, USMBA University Fez, Morocco
[b] Laboratory of Electrical Engineering and Maintenance, Higher School of Technology, University Mohammed I Oujda, Morocco

HIGHLIGHTS

- Nonlinear model guarantee reaching the optimal solution.
- It is compared to similar control methods to prove its effectiveness.
- Efficiency affirmation by an experimental control validation test.
- Simulation experiments on the Simulink platform and validation on the dSPACE board controller are conducted.

ARTICLE INFO

Article history:
Received 16 March 2019
Received in revised form 20 June 2019
Accepted 27 June 2019
Available online xxxx

Keywords:
WECS
PMSG
dSPACE 1104
PWM
Backstepping control
Matlab–Simulink

ABSTRACT

This paper describes the design and implementation in real time of a nonlinear control for a wind energy conversion system (WECS). The Backstepping control has been implemented to improve the performance of the conversion system based on a permanent magnet synchronous generator (PMSG) connected to the grid. Two static back-to-back converters ensure grid connection and are controlled by Pulse Width Modulation (PWM). The proposed control algorithm ensures proper speed control to extract maximum power. First of all, a WECS full review has been discussed. Thereafter, a Backstepping control laws detailed description based on the Lyapunov stability technique has been reported. Consequently, these control thus helping it possible to operate the complete system in the best performances in the static and dynamic regimes. The second part of this article has been devoted to the Backstepping control experimental validation using the dSPACE DS1104 control board and the Matlab–Simulink environment in order to check and validate the system efficiency. The results achieved have been clearly responded to the requirements of robustness and follow-up of references even under fluctuating wind conditions, and confirmed the control effectiveness in both static and dynamic operating modes.

© 2019 The Authors. Published by Elsevier Ltd. This is an open access article under the CC BY-NC-ND license (http://creativecommons.org/licenses/by-nc-nd/4.0/).

1. Introduction

In recent years, a serious awareness to the preservation of the globe and the environment is strongly exhibited. Most countries have engaged in this dynamic to reduce the problems of greenhouse gas emissions. In this context and among the strategies involved, we find the renewable energies integration in order to guarantee a sustainable development and this without compromising the natural resources of future generations (Dogan and Seker, 2016). However, the renewable energy sector is becoming more competitive because of the gradual demand for energy (Kannan and Vakeesan, 2016; Ahmed et al., 2016; Lund and Boyd, 2016; Huang et al., 2018; Fallahzadeh-Abarghouei et al., 2018; El Mourabit et al., 2017; Domínguez-Navarro et al., 2019; Dragomir et al., 2016; Pacesila et al., 2016; Alemany et al., 2018). In addition, wind energy technology has positioned itself as the biggest growing in the world and considers itself as the future energy (Dragomir et al., 2016).

However, these known technologies have a disadvantages number which makes the energy costs too high, among other things, the energy produced from the wind. For this reason, it is important to put smarter systems that meet the requirements of integrating power generation into the grid (Islam et al., 2013; Mahela and Shaik, 2016; Pacesila et al., 2016; Abbasi and Abbasi, 2016). On the other hand, global electricity production based on wind energy reached 600.278 GW in 2018 against 546.388 GW in 2017, an increase of 53,89 GW which representing a rate of

* Corresponding author.
E-mail address: youness.elmourabit@usmba.ac.ma (E.M. Youness).

https://doi.org/10.1016/j.egyr.2019.06.015
2352-4847/© 2019 The Authors. Published by Elsevier Ltd. This is an open access article under the CC BY-NC-ND license (http://creativecommons.org/licenses/by-nc-nd/4.0/).

Nomenclature

Active generator power	P_{gen} (W)
Active grid power	P_g (W)
Blade swept area	S (m^2)
Controller parameters	K_d, K_q, K_Ω (–)
DC-link voltage	V_{DC} (V)
d-q axis flux	Ψ_d, Ψ_q (Wb)
d-q axis inductance	L_d, L_q (H)
d-q axis grid current	i_{gd}, i_{gq} (A)
d-q axis grid voltage	V_{gd}, V_{gq} (V)
d-q axis stator current	i_{sd}, i_{sq} (A)
d-q axis stator voltage	V_{sd}, V_{sq} (V)
Electric pulsation	ω_r (rad/s)
Electromagnetic generator torque	T_{em} (N · m)
Generator flux	$\varnothing_f$ (Wb)
Grid pulsation	ω_g (rad/s)
Grid side converter voltage	V_{id}, V_{iq} (V)
Laplace magnitude	p (-)
Mechanical generator speed	Ω_{mec} (rpm)
Mechanical turbine speed	Ω_t (rpm)
Number of poles pairs	P (-)
Optimal turbine torque	T_{tur}^{opt} (N·m)
pitch angle	β (°)
Power captured by the wind turbine	P_t (W)
Power coefficient	C_p (–)
Radius of the turbine blade	R (m)
Reactive generator power	Q_{gen} (var)
Reactive grid power	Q_g (var)
Reference generator torque	T_{em_ref} (N·m)
Specific density of air	ρ (Kg/m^3)
Stator voltage vector	V_s (V)
Stator resistance	R_s (Ω)
Time	t (S)
tip-speed ratio	λ (-)
Turbine torque	T_{tur} (N·m)
Wind speed	V_w (m/s)

+9.86% (Global Wind Energy Council (GWEC), 2017) as shown in Fig. 1.

The new control concepts necessity for wind energy conversion system is becomes paramount for the power generation ideal operating safety. However, a good mastery of the WECS architecture and wind turbines leads to best energy yields (Tummala et al., 2016). It was for this purpose, scientific researchers are continually developing new wind turbine generator control algorithms to reduce installation costs and improve energy efficiency (Cheng and Zhu, 2014).

Nonetheless, wind farms have become complex systems that require the new control application to guarantee optimum energy efficiency (Taoussi et al., 2016; Bossoufi et al., 2014a; Ionita, 2012; Bossoufi et al., 2014b). The appearance of high-performance digital computers and technological advances offers an immense evolution of electrical machine control techniques. One finds among other things the nonlinear control Backstepping (Rezaei, 2018).

In this context, the set objective through this paper focuses on impact assessment of the Backstepping control applied to the WECS which is based on PMSG. Of course, this generator presents an optimal choice in the future thanks to its multiple qualities compared to other AC generators. Indeed, the PMSG takes its place in the wind farm market at present due to its high efficiency, its high power density, its robustness and its weight which remains considerably weak compared to asynchronous generators of the same power (Chen et al., 2009). Another important reason that leads to this choice is due to the manufacturing design of this generator. Truly, this generator is designed to work with low rotational speeds and therefore adapts to the low wind profile. This design is based on the PMSG arrangement of a large number of poles which facilitates the angular speed adaptation in relation to the wind speed (Pareta and Sen, 2014). This great competitive advantage replaces the wind turbines gearbox based on asynchronous generators, which subsequently eliminates the mechanical defects and the maintenance required for this type installation.

The PMSG control remains considerably complex because of several factors. As an example, the non-linearity of the generator analytical model, a highly coupled and multi-variable machine, sensitive to parametric variations and disturbances of the external environment elements. That to this vision, researchers are continuing to improve the control algorithms that have been developed to perform decoupled PMSG control and improve the performance of the complete WECS.

Decoupling at the PMSG is accomplished by applying control algorithms. Among these algorithms lies the theory of Field oriented control (FOC), or strictly speaking, the vector control. This command, which was founded in 1971 by Blaschke, consists in decoupling the torque control from that of the flux while directing the flux along an appropriate mark axis (El Ouanjli et al., 2019). The FOC control is based on conventional controllers PI in combination with compensation terms to decouple the current into two axes direct and quadrature. The quadrature axis will be used for torque setting and the direct axis will be used for flux adjustment. But the disadvantages of this control lie essentially in the sensitivity to machine parametric variations. This can cause harmful errors and lead to degradation system performance.

To improve the FOC failure and replace conventional control techniques, the nonlinear Backstepping control is presented in this work and seeks to make a global stability of the studied system. Indeed, this nonlinear control algorithm based on the Lyapunov stability technique offers better results without using the analytical models of generator and system. Certainly, this control algorithm does not depend on the generator parameters essential for the FOC control, and therefore does not require any parametric identification for possible regulation.

This document has set an implement objective a real-time nonlinear Backstepping control at a permanent magnet synchronous generator, piloted by voltage inverters. It also aims to control and to order the WECS through the dSPACE 1104 board for different wind conditions. In order to properly situate this work, the contribution made through this paper is focused on the following points:

- Ensure optimal operation for the WECS based on PMSG while applying nonlinear control.
- Ensure the benefits of FOC and overcome its disadvantages in various simulation situations.
- Adopt a Backstepping control law based on Lyapunov's stability theory to improve the system overall performance in response to changes in external elements.
- Validate and prove the Backstepping control effectiveness under different wind profiles using the real time dSPACE 1104 control board.

This article is structured in six sections: Section 1 is an introduction. Section 2 provides a brief literature review of the recent

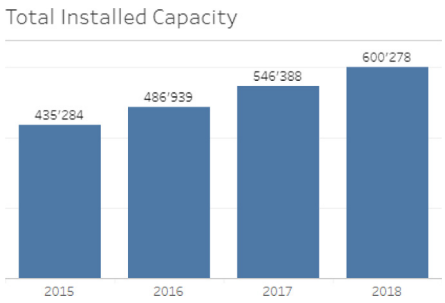

Fig. 1. Global cumulative installed wind power capacity (in megawatts) (Global Wind Energy Council (GWEC), 2017).

studies of adaptive controls applied to WECS. Section 3 describes the wind energy conversion system modeling. Section 4 presents the Backstepping command based on the Lyapunov stability technique with a control laws detailed analysis. Section 5 will be reserved to the simulation results found and the experimental validation and their interpretations will be presented in Section 6. Finally a main conclusion of this work summarizes and proves the Backstepping control validity.

2. Literature review

2.1. Recent studies on adaptive control in wind energy systems

To achieve robust controls of electrical machines that generally overcomes the conventional controls failures. Many researchers are constantly developing new complex control algorithms that take account of the difficulties associated with machine model nonlinearities. Among these control algorithms we cite: the Backstepping control, Sliding Mode Control (SMC), Adaptive Second Order Sliding Mode Control (SOSMC). This brief study presents publications of some control algorithms used in the wind energy conversion system.

Benakcha et al. (2018) presented a comparison between two controls of a wind energy conversion system based on Dual Stator Induction Generator DSIG, one focuses on the classical PI controllers and the other is based on a nonlinear Backstepping control. The authors proved that the Backstepping control makes the difference and the system improvement in transient mode is at the rapidity or the overshoot.

The authors in Errami et al. (2015) put a comparison between the PMSG sliding mode controls with classical PI controllers. Two PMSG of 2 MW each form a wind farm the interest of this study. The objective set through the document serves to maximize the power extracted from the wind under different situations and change of external elements. The results achieved clearly show the improvement brought by the nonlinear control SMC in the two static and dynamic modes of system.

Bossoufi et al. (2015) worked on the adaptive control Backstepping of DFIG to control a wind energy conversion system. The use of the FPGA card is a solution provided for the practical validation of a wind emulator based on a DFIG of 200 KW. The robustness and reliability of the proposed nonlinear control are proven according to the achieved results in presence of a fluctuating wind profile.

Fantino et al. (2016) presented a work of PMSG speed measurement without using mechanical sensors. It is indeed a Luenberger nonlinear observer and this from the electrical quantities. The control laws employed prove the effectiveness of the nonlinear observer-based strategy for a speed estimate in order to control the machine electromagnetic torque.

Rezaei (2018) proposed adaptive nonlinear Backstepping control to follow the maximum power point of a DFIG based wind turbine. This command is implemented to eliminate the need to use a wind speed sensor in the MPPT algorithm. The DFIG Backstepping control put laws that do not require knowledge of the machine parametric characteristics. The results found by simulation clearly show the control effectiveness against parametric variations and wind speed changes.

Matraji et al. (2018) unveiled the effectiveness of a second-order sliding mode control algorithm (SOSMC). A PMSG-based wind emulator is being developed to test the action of combining SOSMC with a Super Twisting (ST) algorithm for a wind energy conversion system. The authors also proposed an Adaptive Super Twisting (AST) algorithm to overcome clicking problems. An experimental validation clearly shows the adapted control efficiency.

Table 1 summarizes some appropriate technical for the nonlinear controls used for wind conversion systems.

According to this brief literature study, recent controls applied in WECS are based mainly on induction generators and DFIG. The great-power PMSG has just taken its place in future wind farm projects. The interest through this paper is to apply and validate the nonlinear Backstepping control for a high power PMSG using the dSPACE board. The validation test and the results comparison with other work will be presented along this article to prove the effectiveness provided through this control for PMSG.

3. Wind energy conversion system modeling

The nonlinear Backstepping control development for the WECS based on PMSG requires precise modeling of the machine. That is why the synchronous generator analytical modeling is an essential step. In other words, the analytical model must be the closest to the machine real model in order to have better results later.

The wind energy conversion system structure is represented as shown in Fig. 2.

3.1. Wind Turbine modeling

The goal established by this part will be modeling the WECS aerodynamic aspects. The modeling remains simple either at the level of the wind profile or wind turbine models.

The wind kinetic energy conversion into mechanical energy is ensured by a turbine. Moreover, the kinetic energy stored in the air is proportional to the unit area perpendicular to the wind speed direction.

Wind power (P_{wind}) is presented by Zhang et al. (2011):

$$P_{wind} = \frac{1}{2} \cdot \rho \cdot S \cdot V_{w^3} \tag{1}$$

Into account the blades aerodynamics, the power extracted by a wind turbine only presents a part of the power available to the wind. This extracted power can be written:

$$P_t = C_p(\lambda, \beta) * P_{wind} = \frac{1}{2} \cdot C_p(\lambda, \beta) \cdot \rho \cdot S \cdot V_{w^3} \tag{2}$$

Where C_p represents a report known as the Betz limit. The power coefficient C_p makes it possible to express the efficiency of the wing to extract mechanical energy from the wind kinetic energy. This coefficient depends on the pitch angle (β) and the tip speed ratio known as the TSR indicated by (λ) (Sun et al., 2003):

$$\begin{cases} \frac{1}{\lambda'} = \frac{1}{\lambda + 0.08\beta} - \frac{0.035}{\beta^3 + 1} \\ C_p(\lambda, \beta) = c_1\left(\frac{c_2}{\lambda'} - c_3\beta - c_4\right)e^{\frac{-c_5}{\lambda'}} + c_6\lambda \end{cases} \tag{3}$$

Table 1
Adaptive control in renewable wind energy systems.

Techniques	Researchers
Nonlinear observer	Fantino et al. (2016); Shotorbani et al. (2019)
Backstepping control	Rezaei (2018); Benakcha et al. (2018); Bossoufi et al. (2015); Kortabarria et al. (2014); Nemmour et al. (2010); Bossoufi et al. (2014b); Bektache and Boukhezzar (2018); Yang et al. (2016)
Sliding Mode Control (SMC)	Domínguez-Navarro et al. (2019); Errami et al. (2015); Mérida et al. (2014); Liu et al. (2018); Prasad et al. (2019); Djoudi et al. (2018); Zamzoum et al. (2019)
Adaptive Second (High)-Order Sliding Mode Control (SOSMC-HOSMC)	Matraji et al. (2018); Xiong et al. (2019); Benbouzid et al. (2014)

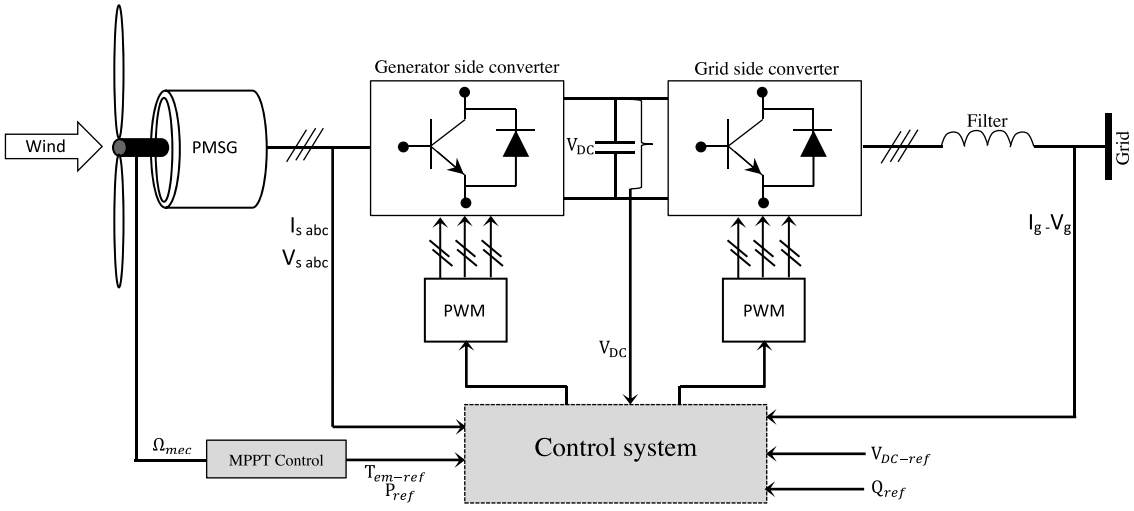

Fig. 2. General model of WECS.

Table 2
Aerodynamic constants of a considered wind turbine.

Parameters	Coefficients
C_1	0.5176
C_2	116
C_3	0.4
C_4	5
C_5	21
C_6	0.0068

Where, β represents the blade pitch angle in degrees. The parameters C_1, C_2, C_3, C_4, C_5 and C_6 are constants dependent on the turbine geometry (see Table 2).

The reduced speed λ can be defined by the following relation:

$$\lambda = \frac{R \cdot \Omega_t}{V_w} \tag{4}$$

According to Eqs. (2) and (4) we can draw the turbine torque formula. The torque is proportional to the square of the rotor angular speed as shown by the following relation:

$$T_{tur} = \frac{1}{2} \cdot \frac{C_p(\lambda) \cdot \rho \cdot S \cdot R^3}{\lambda^3} \cdot \Omega_t^2 = \frac{1}{2} \cdot \rho \cdot \pi \cdot R^2 \cdot C_p \cdot \frac{V_w^3}{\Omega_t} \tag{5}$$

According to Eq. (3), the plot of power coefficient C_p is as shown in Fig. 3. This plot is in function according to several values of λ and β.

In ideal case, the power coefficient C_p reaches a maximum value that will be within the range 59.26% according to Betz's limit.

3.2. PMSG modeling

The permanent magnet synchronous generator is the center of the wind energy conversion plant for this study. The PMSG is chosen because of its many advantages. The dynamic equations governing the PMSG operation will be presented in a synchronous rotating reference frame (d-q) as follows (Hong et al., 2013):

- Stator voltages:
$$\begin{cases} V_{sd} = R_s \cdot i_{sd} + \dfrac{d\Psi_d}{dt} - \omega_r \cdot \Psi_q \\ V_{sq} = R_s \cdot i_{sq} + \dfrac{d\Psi_q}{dt} + \omega_r \cdot \Psi_d \end{cases} \tag{6}$$
- Stator fluxes:
$$\begin{cases} \Psi_d = L_d \cdot i_{sd} + \Phi_f \\ \Psi_q = L_q \cdot i_{sq} \end{cases} \tag{7}$$

This allows writing:

$$\begin{cases} V_{sd} = R_s \cdot i_{sd} + L_d \dfrac{di_{sd}}{dt} - \omega_r \cdot L_q \cdot i_{sq} \\ V_{sq} = R_s \cdot i_{sq} + L_q \dfrac{di_{sq}}{dt} + \omega_r \cdot L_d \cdot i_{sd} + \omega_r \cdot \Phi_f \end{cases} \tag{8}$$

The PMSG equivalent circuit in the rotating reference system d-q is represented in Fig. 4.

The electromagnetic torque expression in the Park coordinate system and the mechanical equation describe the system are given by:

$$\begin{cases} T_{tur} - T_{em} = J \cdot \dfrac{d\Omega}{dt} + f_c \cdot \Omega \\ T_{em} = \dfrac{3}{2} \cdot p \cdot \left[\left(L_d - L_q \right) i_{sd} \cdot i_{sq} + i_{sq} \cdot \Phi_f \right] \end{cases} \tag{9}$$

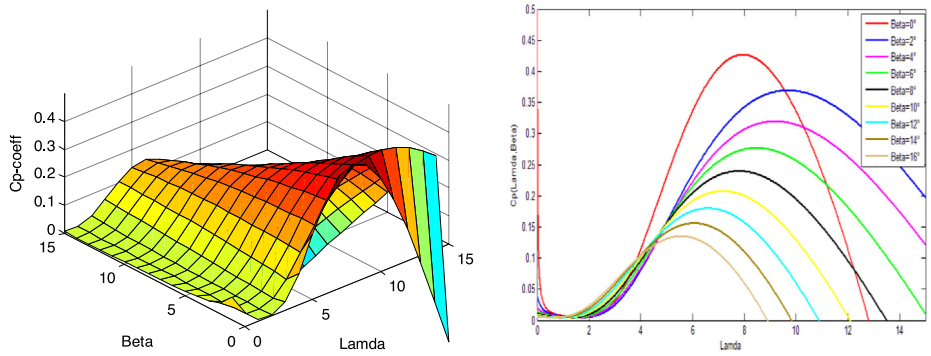

Fig. 3. Coefficient of performance C_p with TSR (λ) for several pitch angles (β).

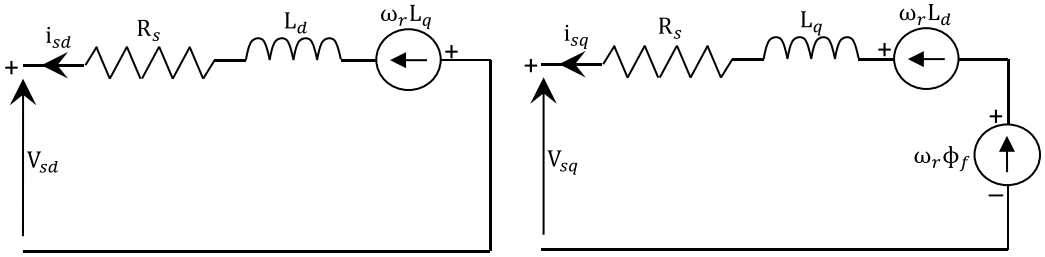

Fig. 4. *d-q* model of PMSG in synchronous reference frame.

Moreover, the active and reactive powers expressions can be calculated according to the following equations:

$$\begin{cases} P_{gen} = \dfrac{3}{2}\left[V_{sd}\cdot i_{sd} + V_{sq}\cdot i_{sq}\right] \\ Q_{gen} = \dfrac{3}{2}\left[V_{sq}\cdot i_{sd} + V_{sd}\cdot i_{sq}\right] \end{cases} \tag{10}$$

4. Backstepping control applied to WECS

4.1. Generator side converter control

4.1.1. Backstepping control strategy

The nonlinear systems control domain requires high-performance algorithms to ensure a better level of stability and performance. The Backstepping control is part of the algorithms in this area. This technique, which was developed by Kanellakopoulos in 1990, offers a systematic method for producing controllers for nonlinear systems (Kanellakopoulos et al., 1991). The Backstepping strategy charged to make a representation using several subsystems order 1 that is cascaded to disassociate the overall system. Each subsystem provides a virtual command for the next subsystem to ensure the process convergence to its equilibrium state. In this context, we find Lyapunov functions that ensure the system overall stability.

4.1.2. Description model

The PMSG is modeled according to Eqs. (8) and (9), it can clearly be seen that this model is strongly nonlinear because of the coupling between electric currents and speed. The purpose is to apply the Backstepping to control the machine-side converter by reference voltages. For this, we will consider the stator currents and the mechanical speed as state variables and the stator voltages as control variables.

The machine can be again represented as follows:

$$\begin{cases} \dfrac{di_{sd}}{dt} = \dfrac{1}{L_d}\left(-R_s\cdot i_{sd} + p\cdot\Omega\cdot L_q\cdot i_{sq} + V_{sd}\right) \\ \dfrac{di_{sq}}{dt} = \dfrac{1}{L_q}\left(-R_s\cdot i_{sq} - p\cdot\Omega\cdot L_d\cdot i_{sd} - p\cdot\Omega\cdot\Phi_f + V_{sq}\right) \\ \dfrac{d\Omega}{dt} = \dfrac{1}{J}\left(T_{tur} - T_{em} - f_c\cdot\Omega\right) \end{cases} \tag{11}$$

In order to obtain operation with maximum electromagnetic torque, it is enough to force the direct stator current to zero. Then we will choose the current reference $i_{sd-ref} = 0$. Regulating the current isd to a reference value isd-ref equal to zero allows guaranteeing the absence of *d*-axis stator current, implying thus no reluctance torque. Doing so, only the *q*-axis reactance is involved in producing the final voltage, i.e., there is no direct magnetization or demagnetization of *d*-axis, only the field winding contributes to producing the flux along this direction. It also guarantees a gain in the reference electromagnetic torque.

$$\begin{cases} V_{sd} = -p\cdot\Omega\cdot L_q\cdot i_{sq} \\ \dfrac{di_{sq}}{dt} = \dfrac{1}{L_q}\left(-R_s\cdot i_{sq} - p\cdot\Omega\cdot\Phi_f + V_{sq}\right) \end{cases} \tag{12}$$

The electromagnetic torque becomes:

$$T_{em\_opt} = \frac{3}{2}\cdot p\cdot i_{sq}\cdot\Phi_f \tag{13}$$

The strategy subsequently applied decomposes down into two consecutive stages. The first step provides the necessary instructions for the second step. The control vectors are chosen so that $[x] = [x_1x_2x_3]^T = [i_{sd}i_{sq}\Omega]^T$ as state vectors and u=[V $_{sd}$ V_{sq}]^T as a control vector.

■ Step1: Backstepping speed controller

The tracking error of the state variable x_3 can be defined by:

$$\xi_\Omega = \Omega_{ref} - \Omega \tag{14}$$

This offers as speed error dynamics:

$$\dot{\xi_\Omega} = \frac{d\xi_\Omega}{dt} = \dot{\Omega}_{ref} - \dot{\Omega} = \dot{\Omega}_{ref} - \frac{1}{J}\left[T_{tur} - \frac{3p}{2}\left(\left(L_d - L_q\right)\cdot i_{sd}\cdot i_{sq} + i_{sq}\cdot\Phi_f\right) - f_c\cdot\Omega\right] \tag{15}$$

The first step guarantees a follow-up of the reference speed and consequently makes it possible to annul the speed error. Lyapunov's function is used for this purpose.

$$V_1 = \frac{1}{2}\cdot\xi_\Omega^2 \tag{16}$$

The Lyapunov function derivative is therefore:

$$\dot{V}_1 = \xi_\Omega\cdot\dot{\xi_\Omega} = -K_\Omega\xi_\Omega^2 + \frac{\xi_\Omega}{J}\left(-T_{tur} + f_c\cdot\Omega + K_\Omega\cdot J\cdot\xi_\Omega + \frac{3}{2}\cdot p\cdot i_{sq}\cdot\Phi_f\right) + \frac{3}{2J}\cdot p\cdot\left(L_d - L_q\right)\cdot i_{sd}\cdot i_{sq}\cdot\xi_\Omega \tag{17}$$

We must choose negative $\dot{V}_1$ to ensure the first subsystem stability. This results in the correct choice of the stator currents values i_{sd} and i_{sq}.

$$\begin{cases} i_{sd-ref} = 0 \\ i_{sq-ref} = \dfrac{2}{3\cdot p\cdot\Phi_f}\left(T_{tur} - f_c\cdot\Omega - K_\Omega\cdot J\cdot\xi_\Omega\right) \end{cases} \tag{18}$$

We will replace the equation elements (18) in Eq. (17) with $\dot{\Omega}_{ref} = 0$:

$$\dot{V}_1 = -K_\Omega\xi_\Omega^2 \le 0 \tag{19}$$

The system described by Eq. (11) will be stable if one chooses k_Ω positive constant.

■ Step2: Backstepping current controller

The second step of this algorithm resides on the control voltages calculation V_{sd} and V_{sq} which will be calculated based on the system virtual inputs. The stator currents i_{sd} and i_{sq} which are chosen as virtual inputs will have as errors:

$$\begin{cases} \xi_d = i_{sd-ref} - i_{sd} \\ \xi_q = i_{sq-ref} - i_{sq} \end{cases} \tag{20}$$

Based on Eqs. (18) and (20), the speed dynamic calculated in (15) becomes:

$$\begin{aligned} \dot{\xi_\Omega} &= \frac{d\xi_\Omega}{dt} \\ &= \frac{1}{J}\left[-T_{tur} + f_c\cdot\Omega + \frac{3p}{2}\left(\left(L_d - L_q\right)\cdot i_{sd}\cdot i_{sq} + i_{sq}\cdot\Phi_f\right)\right] \\ &= \frac{1}{J}\left[-T_{tur} + f_c\cdot\Omega + \frac{3p}{2}\Phi_f\cdot\left(i_{sq-ref}\right) - \frac{3p}{2}\cdot\left(L_d - L_q\right)\cdot i_{sq}\cdot\xi_d\right] \\ &= \frac{1}{J}\left[-T_{tur} + f_c\cdot\Omega + \frac{3p}{2}\Phi_f\cdot\left[\frac{2}{3\cdot p\cdot\Phi_f}\left(T_{tur} - f_c\cdot\Omega - K_\Omega\cdot J\cdot\xi_\Omega\right)\right] - \frac{3p}{2}\Phi_f\cdot\xi_q - \frac{3p}{2}\cdot\left(L_d - L_q\right)\cdot i_{sq}\cdot\xi_d\right] \\ &= \frac{1}{J}\left[-K_\Omega\cdot J\cdot\xi_\Omega - \frac{3p}{2}\Phi_f\cdot\xi_q - \frac{3p}{2}\cdot\left(L_d - L_q\right)\cdot i_{sq}\cdot\xi_d\right] \end{aligned} \tag{21}$$

From Eqs. (11) and (20) the calculation of the currents errors dynamics gives:

$$\begin{cases} \dot{\xi_d} = \dot{i_{sd-ref}} - \dot{i_{sd}} \\ \dot{\xi_q} = \dot{i_{sq-ref}} - \dot{i_{sq}} \end{cases} \tag{22}$$

$$\dot{\xi_d} = \dot{i_{sd-ref}} - \dot{i_{sd}} = 0 - \dot{i_{sd}} = -\frac{di_{sd}}{dt} = \frac{1}{L_d}\left(R_s\cdot i_{sd} - p\cdot\Omega\cdot L_q\cdot i_{sq} - V_{sd}\right) \tag{23}$$

$$\begin{cases} \dot{\xi_q} = \dot{i_{sq-ref}} - \dot{i_{sq}} = \frac{2}{3\cdot p\cdot\Phi_f}\left(-f_c\cdot\dot{\Omega} - K_\Omega\cdot J\cdot\dot{\xi_\Omega}\right) + \frac{1}{L_q}\left(R_s\cdot i_{sq} + p\cdot\Omega\cdot L_d\cdot i_{sd} + p\cdot\Omega\cdot\Phi_f - V_{sq}\right) \\ \quad = \dfrac{2}{3\cdot p\cdot\Phi_f}\left(-f_c\cdot\dfrac{1}{J}\left(T_{tur} - T_{em} - f_c\cdot\Omega\right) - K_\Omega\cdot J\cdot\dfrac{1}{J}\left[-T_{tur} + f_c\cdot\Omega + \dfrac{3p}{2}\left(\left(L_d - L_q\right)\cdot i_{sd}\cdot i_{sq} + i_{sq}\cdot\Phi_f\right)\right]\right) \\ \qquad + \dfrac{1}{L_q}\left(R_s\cdot i_{sq} + p\cdot\Omega\cdot L_d\cdot i_{sd} + p\cdot\Omega\cdot\Phi_f - V_{sq}\right) \\ \quad = \frac{2}{3\cdot p\cdot J\cdot\Phi_f}\left(-f_c\cdot\left(T_{tur} - \frac{3p}{2}\left(\left(L_d - L_q\right)\cdot i_{sd}\cdot i_{sq} + i_{sq}\cdot\Phi_f\right) - f_c\cdot\Omega\right) + K_\Omega\cdot J\cdot\left[T_{tur} - f_c\cdot\Omega - \frac{3p}{2}\left(\left(L_d - L_q\right)\cdot i_{sd}\cdot i_{sq} + i_{sq}\cdot\Phi_f\right)\right]\right) \\ \qquad + \dfrac{1}{L_q}\left(R_s\cdot i_{sq} + p\cdot\Omega\cdot L_d\cdot i_{sd} + p\cdot\Omega\cdot\Phi_f - V_{sq}\right) \\ \quad = \dfrac{2}{3\cdot p\cdot J\cdot\Phi_f}\left(\left(K_\Omega\cdot J - f_c\right)\left[T_{tur} - f_c\cdot\Omega - \dfrac{3p}{2}\left(\left(L_d - L_q\right)\cdot i_{sd}\cdot i_{sq} + i_{sq}\cdot\Phi_f\right)\right]\right) \\ \qquad + \dfrac{1}{L_q}\left(R_s\cdot i_{sq} + p\cdot\Omega\cdot L_d\cdot i_{sd} + p\cdot\Omega\cdot\Phi_f - V_{sq}\right) \end{cases} \tag{24}$$

As long as the system becomes somewhat complex and contains three state variables, we are forced to choose a second Lyapunov function which taken into consideration the errors of the stator currents and rotation speed. The voltages V_{sd} and V_{sq} will be the control voltages for the machine-side converter.

First defining the Lyapunov function:

$$V_2 = \frac{1}{2}\left(\xi_\Omega^2 + \xi_d^2 + \xi_q^2\right) \tag{25}$$

Using Eqs. (21), (23) and (24), the second Lyapunov function derivative becomes:

$$\dot{V}_2 = \left(\xi_\Omega\dot{\xi_\Omega} + \xi_d\dot{\xi_d} + \xi_q\dot{\xi_q}\right) \tag{26}$$

$$\begin{cases} \dot{V}_2 = -K_\Omega\xi_\Omega^2 - K_d\xi_d^2 - K_q\xi_q^2 \\ \quad + \dfrac{\xi_\Omega}{J}\left(-\dfrac{3p}{2}\cdot\Phi_f\cdot\xi_q - \dfrac{3p}{2}\cdot\left(L_d - L_q\right)\cdot i_{sq}\cdot\xi_d\right) \\ \quad + \dfrac{\xi_d}{L_d}\left(R_s\cdot i_{sd} - p\cdot\Omega\cdot L_q\cdot i_{sq} - V_{sd} + K_d\cdot L_d\cdot\xi_d\right) \\ \quad + \dfrac{\xi_q}{L_q}\left[\dfrac{2\cdot L_q}{3\cdot p\cdot J\cdot\Phi_f}\left(\left(K_\Omega\cdot J - f_c\right)\left[T_{tur} - f_c\cdot\Omega - \dfrac{3p}{2}\left(\left(L_d - L_q\right)\cdot i_{sd}\cdot i_{sq} + i_{sq}\cdot\Phi_f\right)\right]\right) + R_s\cdot i_{sq} + p\cdot\Omega\cdot L_d\cdot i_{sd} + p\cdot\Omega\cdot\Phi_f - V_{sq} + K_q\cdot L_q\cdot\xi_q\right] \end{cases} \tag{27}$$

In order to ensure a system stability one must choose the constants k_d and k_q of the positive constants. On the other hand, the Lyapunov function derivative will be negative if we impose

as reference voltages:

$$\begin{cases} V_{sd-ref} = R_s \cdot i_{sd} - p \cdot \Omega \cdot L_q \cdot i_{sq} + K_d \cdot L_d \cdot \xi_d \\ \qquad - \dfrac{3p}{2 \cdot J} \cdot L_d \cdot \left(L_d - L_q\right) \cdot i_{sq} \cdot \xi_\Omega \\ V_{sq-ref} = \dfrac{2 \cdot L_q}{3 \cdot p \cdot J \cdot \Phi_f} \left(\left(K_\Omega \cdot J - f_c\right) \left[T_{tur} - f_c \cdot \Omega \right. \right. \\ \qquad \left. \left. - \dfrac{3p}{2} \left(\left(L_d - L_q\right) \cdot i_{sd} \cdot i_{sq} + i_{sq} \cdot \Phi_f \right) \right] \right) \\ \qquad + R_s \cdot i_{sq} + p \cdot \Omega \cdot L_d \cdot i_{sd} + p \cdot \Omega \cdot \Phi_f + K_q \cdot L_q \cdot \xi_q \\ \qquad - \dfrac{3p}{2 \cdot J} \cdot L_q \Phi_f \cdot \xi_\Omega \end{cases} \tag{28}$$

4.2. Grid side converter control

In order to maintain the DC bus voltage constant and to ensure an energy good transfer to the distribution grid, it is necessary to control the GSC.

The grid voltages in the d-q referential can be represented as follows:

$$\begin{cases} V_{gd} = V_{id} - R_g \cdot i_{gd} - L_g \cdot \dfrac{d\left(i_{gd}\right)}{dt} + \omega_g \cdot \left(L_g \cdot i_{gq}\right) \\ V_{gq} = V_{iq} - R_g \cdot i_{gq} - L_g \cdot \dfrac{d\left(i_{gq}\right)}{dt} - \omega_g \cdot \left(L_g \cdot i_{gd}\right) \end{cases} \tag{29}$$

With, R_g and L_g represent the resistance and the inductance of the filter connected in series.

In other word, the currents dynamics transited to the grid can be defined as shows the equations hereafter:

$$\begin{cases} \dfrac{d\left(i_{gd}\right)}{dt} = \dfrac{V_{id}}{L_g} - \dfrac{R_g}{L_g} \cdot i_{gd} + \omega_g \cdot i_{gq} - \dfrac{V_{gd}}{L_g} \\ \dfrac{d\left(i_{gq}\right)}{dt} = \dfrac{V_{iq}}{L_g} - \dfrac{R_g}{L_g} \cdot i_{gq} - \omega_g \cdot i_{gd} - \dfrac{V_{gq}}{L_g} \end{cases} \tag{30}$$

The module of the grid voltage and current will be defined by the formulas:

$$\left|V_g\right| = \sqrt{\left(V_{gd}\right)^2 + \left(V_{gq}\right)^2} \tag{31}$$

$$\left|i_g\right| = \sqrt{\left(i_{gd}\right)^2 + \left(i_{gq}\right)^2} \tag{32}$$

With R_g, L_g represent respectively the resistance and the reactance of the intermediate filter. i_{gd} and i_{gq} are the direct and quadrature current transited to the grid. ω_g: The grid angular pulsation. V_{id} and V_{iq} the grid side converter voltage components.

The powers components formulas in the rotating referential d-q are given by:

$$P_g = \frac{3}{2}\left(V_{gd} \cdot i_{gd} + V_{gq} \cdot i_{gq}\right) \tag{33}$$

$$Q_g = \frac{3}{2}\left(V_{gq} \cdot i_{gd} - V_{gd} \cdot i_{gq}\right) \tag{34}$$

In order to keep control of the appropriate powers one imposes $V_{gq} = 0$ and $V_{gd} = \left|V_g\right|$. This gives afterwards:

$$P_g = \frac{3}{2}\left(V_{gd} \cdot i_{gd}\right) = \frac{3}{2}\left(\left|V_g\right| \cdot i_{gd}\right) \tag{35}$$

$$Q_g = \frac{3}{2}\left(-V_{gd} \cdot i_{gq}\right) = -\frac{3}{2}\left(\left|V_g\right| \cdot i_{gq}\right) \tag{36}$$

Noting that power control depends mainly on direct and quadrature grid currents. The Backstepping control design by following the above steps.

The first step is to define the currents errors:

$$\begin{cases} \xi_{gd} = i_{gd-ref} - i_{gd} \\ \xi_{gq} = i_{gq-ref} - i_{gq} \end{cases} \tag{37}$$

The errors dynamics gives:

$$\begin{cases} \dot{\xi_{gd}} = -\dot{i_{gd}} \\ \dot{\xi_{gq}} = -\dot{i_{gq}} \end{cases} \tag{38}$$

Calling the Lyapunov function for current errors:

$$V_3 = \frac{1}{2}\left(\xi_{gd}^2 + \xi_{gq}^2\right) \tag{39}$$

After the calculation based on Eqs. (30) and (38) we find the Lyapunov function dynamics as follows:

$$\begin{cases} \dot{V_3} = -K_{gd}\xi_{gd}^2 - K_{gq}\xi_{gq}^2 \\ \qquad + \xi_{gd}\left(\dfrac{V_{id}}{L_g} - \dfrac{R_g}{L_g} \cdot i_{gd} + \omega_g \cdot i_{gq} - \dfrac{V_{gd}}{L_g} + K_{gd} \cdot \xi_{gd}\right) \\ \qquad + \xi_{gd}\left(\dfrac{V_{iq}}{L_g} - \dfrac{R_g}{L_g} \cdot i_{gq} - \omega_g \cdot i_{gd} - \dfrac{V_{gq}}{L_g} + K_{gq} \cdot \xi_{gq}\right) \end{cases} \tag{40}$$

To ensure system stability, gains K_{gd} and K_{gq} will have positive constants. Moreover, the Lyapunov function derivative has to be negative. Consequently, the reference voltages values will be:

$$\begin{cases} V_{id-ref} = R_g \cdot i_{gd} - L_g \cdot \omega_g \cdot i_{gq} - L_g \cdot K_{gd} \cdot \xi_{gd} + V_{gd} \\ V_{iq-ref} = R_g \cdot i_{gq} + L_g \cdot \omega_g \cdot i_{gd} - L_g \cdot K_{gq} \cdot \xi_{gq} + V_{gq} \end{cases} \tag{41}$$

The reference values choice of the direct and quadrature currents will be made from Eqs. (35) and (36). The reference quadrature current value will then be:

$$i_{gq-ref} = -\frac{Q_{g-ref}}{1.5 * V_g} \tag{42}$$

Operation with a unit power factor forces us to put $Q_{g-ref} = 0$. Which implies that the reference value $i_{gq-ref} = 0$. However, the reference current calculation i_{gd-ref} is obtained through the reference bus voltage V_{DC-ref}.

Assuming that the losses in the GSC are neglected we get a power transfer as shown by the following equation:

$$P_g = \frac{3}{2}\left(V_{gd} \cdot i_{gd}\right) = V_{DC} \cdot i_{DC} \tag{43}$$

This allows writing:

$$i_{gd-ref} = \frac{P_{g-ref}}{1.5 * V_{gd}} \tag{44}$$

The nonlinear Backstepping control block diagram is shown in Fig. 5.

5. Results and discussion

In order to test the Backstepping control robustness, we chose the MATLAB–Simulink environment for simulation and the dSPACE 1104 control board for experimental validation. The ruggedness test of control will be done using a wind profile formed as bearings. The follow-up references and energy efficiency will be made using a fluctuating wind profile. The system and machine parameters are shown in Table 5. Moreover, the sampling frequency chosen is 10 kHz.

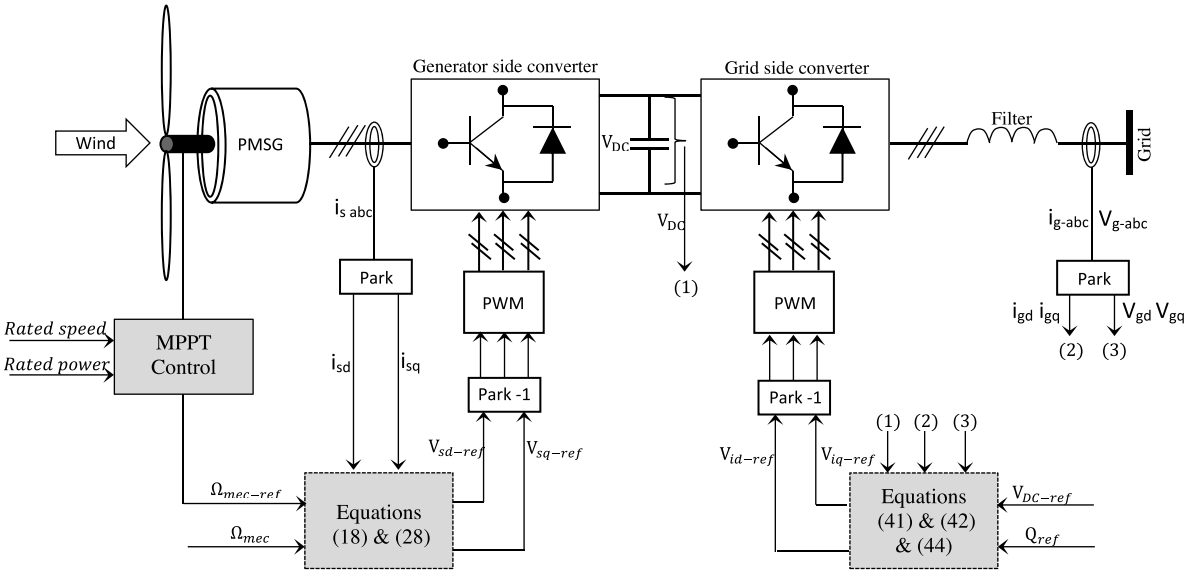

Fig. 5. Backstepping control for WECS.

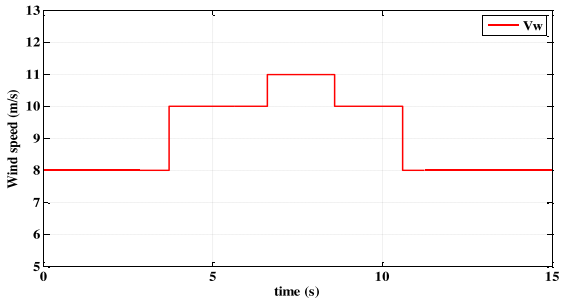

Fig. 6. Ideal wind profile.

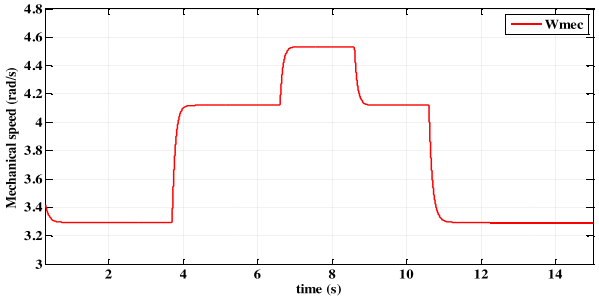

Fig. 7. Mechanical speed.

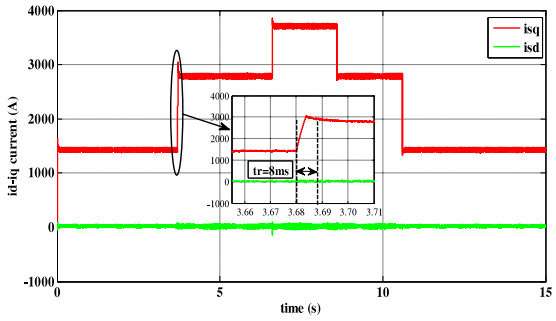

Fig. 8. Stator current $i_{sd} - i_{sq}$.

5.1. Setpoints tracking test simulation

The first test is used to prove the robustness of the Backstepping control on the WECS. It is obvious that the wind profile used for this test does not reflect the real condition; however, this wind profile attests the control chosen performance with respect to the sudden changes of the instructions.

A good functioning of the complete system we must choose the reference direct current $i_{sd-ref} = 0$, which offers maximum electromagnetic torque of the machine with a lesser stator current.

Figs. 6 and 7 respectively represent the results obtained by simulation of the wind profile and the machine angular speed.

The first observation lies in the pace of speed that follows the wind profile evolution in an appropriate manner. Power and currents graphs have the same form as the mechanical speed. The applied Backstepping control offers better performances either at the level of speed or at the level of waves provided quality, it is clearly seen through the currents figures illustrated in Figs. 8 and 9.

The active power form will have the same profile as that of the currents produced by the generator. On the other term, the electrical power tracking with the reference mechanical power is well respected as shown in Fig. 10.

Fig. 11 shows the reactive power evolution with that of its zero reference.

5.2. Simulation of fluctuating wind speed

In order to validate the Backstepping control, a second test with a variable wind profile is implemented. The following figure summarizes the different measurements made previously with the tracking test.

Based on those results, the applied nonlinear control provides good tracking of the setpoints for both the active and reactive power according to Figs. 12(c) and 12(d). The currents generated quality can be observed in both Figs. 12(e) and 12(f).

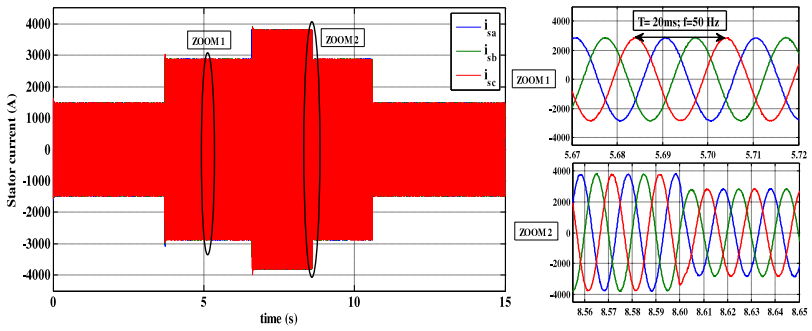

Fig. 9. Injected current i_{abc}.

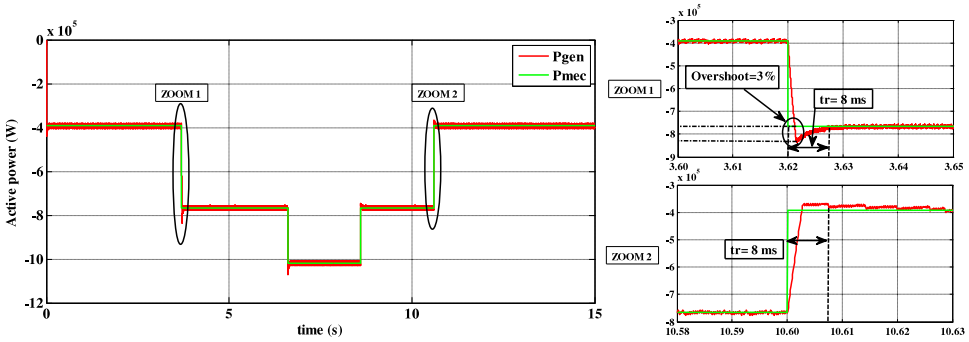

Fig. 10. Generator and mechanical power.

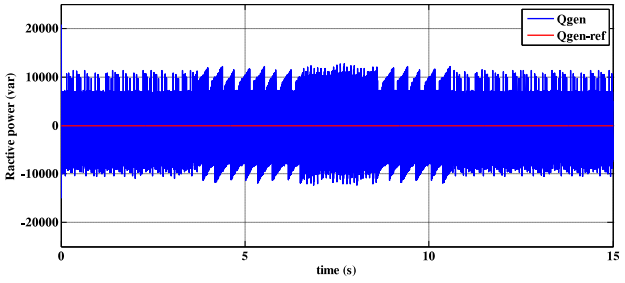

Fig. 11. Reactive power generated.

5.3. Discussion of results

In order to examine the nonlinear Backstepping control performance two tests are applied. The first test enabled us to show and demonstrate the robustness facing the sudden changes in setpoints, while the second test confirms the good follow-up of the variable setpoints.

Operation with zero reactive power provides a regime with a unit power factor. However, negative active power means that the machine is operating in generator mode.

Fig. 10 shows the active power pace with an ideal wind profile. The first observation tired is the speed. A response time in the order to 8 ms is observed in the two graphs Zoom1 and Zoom2 of Fig. 10. The second observation is the overshoot illustrated in Zoom1 of Fig. 10; a rate of 3% for overshoot certifies that even with a significant electrical power the excess rate remains considerably low. The active power follows the turbine mechanical power variation in a perfect manner according to the graphs of Figs. 10 and 12(c). Moreover, the mechanical power varies according to the wind variation. The power low ripple rate is obtained through the waves quality of the currents generated even if for an important power machine. The power performance is around unity. For example, the calculated average mechanical power in the order to (−7.4797e+005 W) and the average electrical power value is around (−7.4796e + 005 W) in the first test, i.e. energy rate of 99.99%. In the second test, the average mechanical value calculated in a period of 50 s is (−4.9675e + 005 W), in addition the average Pgen equal to (−4.9672e + 005 W), which means an energy rate also of 99.99%. In other words, the power error in the first test is 10 W while the error for second test is 30 W. The major finding drawn from these results lies in the good quality of the energy produced by the nonlinear Backstepping control in terms of reliability and energy efficiency.

The reactive power value is kept considerably lower than that of the active power. An average value of 10000 var of the reactive power in the two tests compared with active powers in the order to 400 KW in the second test and can exceed 1 MW in the first test offers optimal operation with a power factor close to one. Effectively, the reactive power in the first test represents only 2.5% compared to the active power value. In the second test, this percentage of Qgen has only 1% of the active power which can exceed 1 MW. In either case, the Backstepping control can keep the reactive power value less than 5% of the total power, which consequently offers a better power factor.

The angular speed shape follows perfectly the set wind profile. The low value of the speed is due to the reason that the machine has a large number of poles. In both tests and regardless of the instructions, the strategy proposed by the Backstepping control offers better tracking and speed performance.

The goal of any control is to provide an electrical currents better quality. This is well seen in graphs 8, 9 and 12(e–f) through nonlinear control. The results obtained from these paces show that the direct stator currents i_{sd} and quadrature i_{sq} perfectly follow the predetermined values. The direct current has a value of zero which offers a maximum electromagnetic torque with a stator current minimum. The quadrature current pace is inversely proportional to the active power supplied. From Fig. 8 it can be observed that the current i_{sq} graph follows fairly rapidly the active

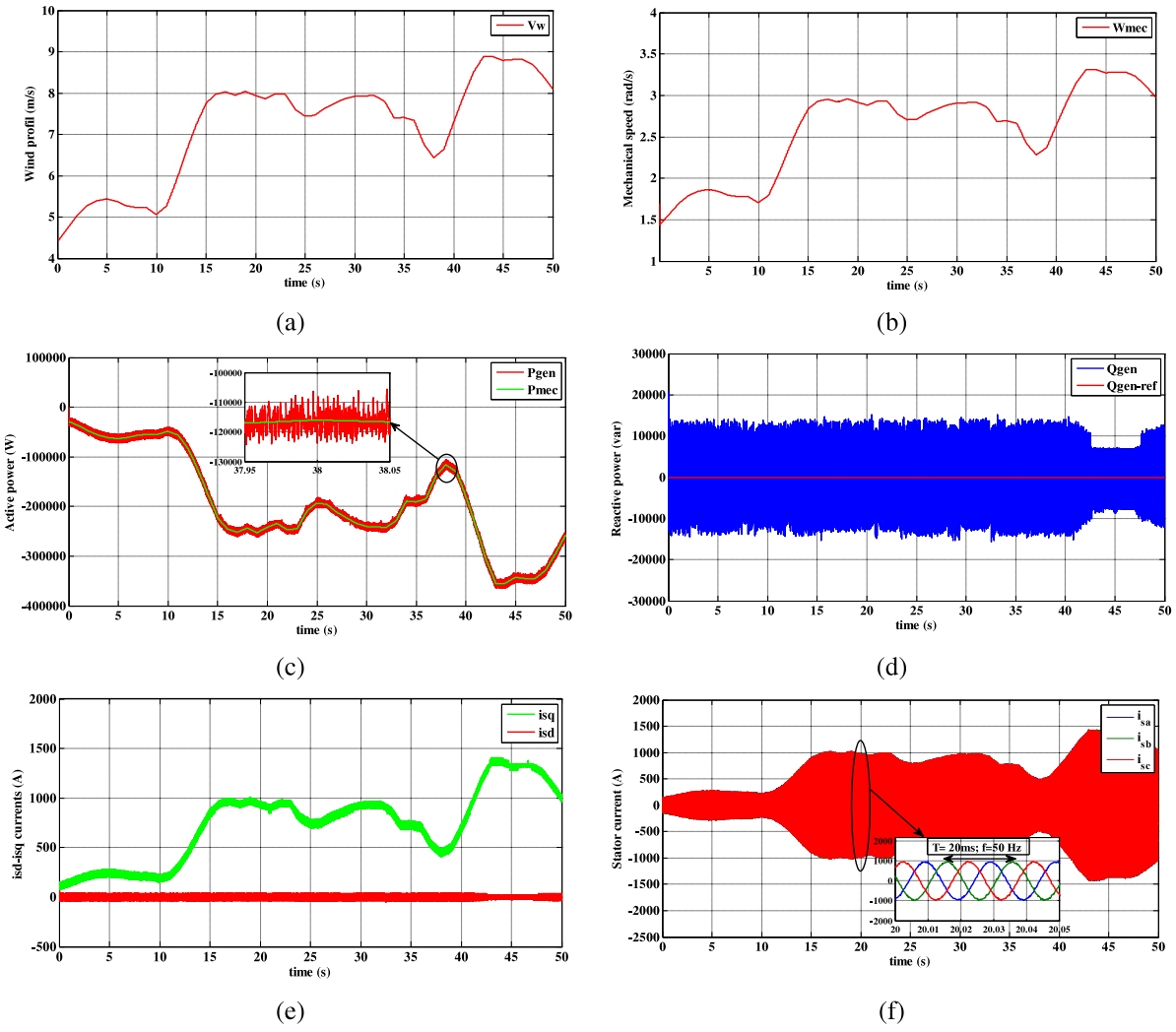

Fig. 12. Fluctuating wind speed figures: (a) Wind profile, (b) Mechanical speed, (c) Active power, (d) Reactive power, (e) Direct and quadrature current, (f) Stator current.

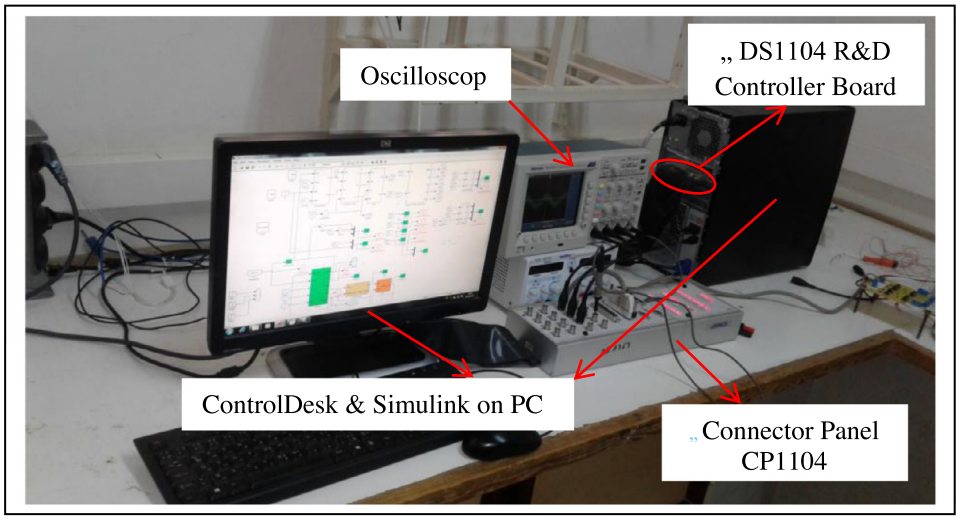

Fig. 13. Real time implementation system.

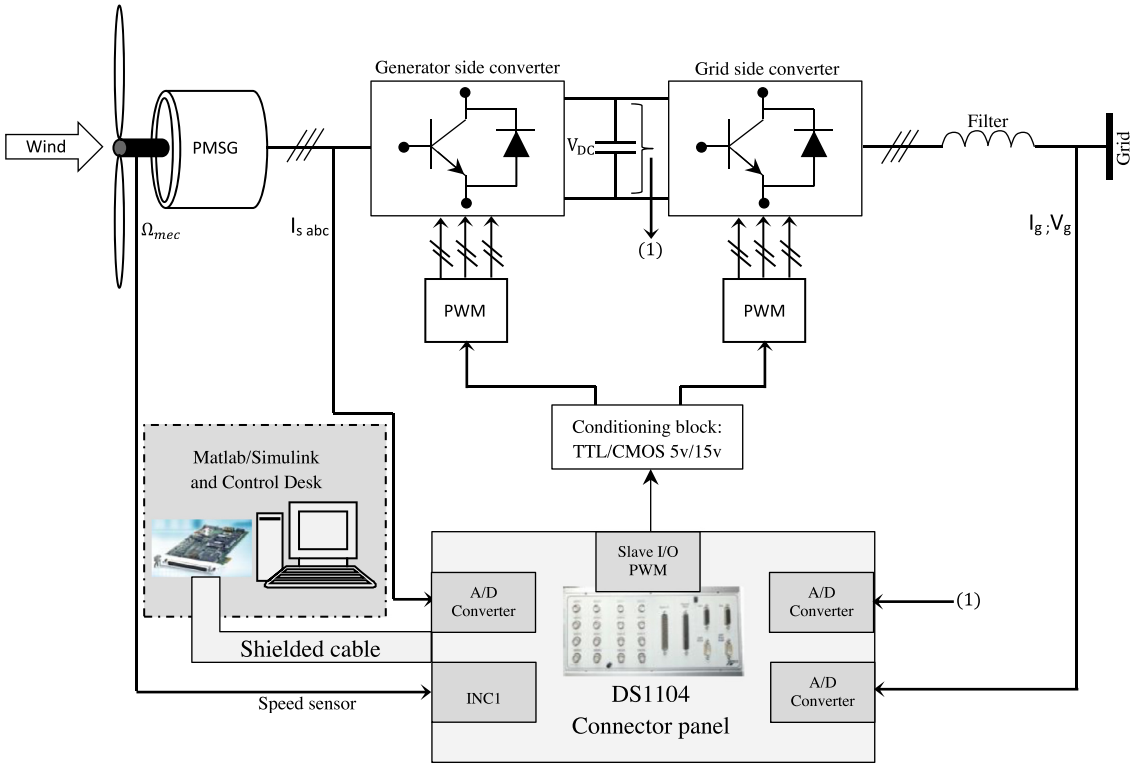

Fig. 14. dSPACE connection scheme with WECS.

power evolution. A 8 ms response time is enough to catch the pursuit.

Fig. 9 illustrates the injected currents pace. The three-phase currents waveform is nearly sinusoidal, reflecting the good quality of electrical energy supplied to the grid. Still in the same Fig. 9 and in the Zoom1 graph, a three-phase waves portion was taken at $t = 5.66$ s. It can be seen that the period of 20 ms which results in a frequency of 50 Hz is well respected. Moreover, a sudden change in power at $t = 8.55$ s leads to such a variation in the injected currents as shown in the Zoom2 graph of Fig. 9. The second observation that can be made is the wave's stability after a very fast catch-up time.

The same remarks are made for the generated currents waves illustrated in Figs. 12(e) and 12(f). The direct stator current for a random wind profile test is always maintained at the null reference ($i_{sd-ref} = 0A$), while the quadrature current is inversely proportional with the active power pace. The three-phase currents shape shown in Fig. 12(e) shows the good quality of the waves even under variable wind conditions. A preview captured at $t = 20$ s clearly shows the quality of energy produced that meets applicable standards. A period of 20 ms and implicitly an adjusted frequency of 50 Hz are respected.

Table 3 summarizes few figures revealed for this simulation in order to validate and prove the performances ensured by the chosen control.

6. Experimental validation

In order to validate the nonlinear Backstepping control performance, a practical solution is being implemented. The control is based on the DS1104 R&D Controller Board developed by dSPACE. This map is enclosed in a computer that ensures the information transfer between the Software and the hardware part. The hardware part of the control board provides both application management and generates PWM control signals in TTL logic 0/5V. Inverters need driver cards to drive IGBTs through slave DSPs TMS320F240 (Anon., 2018). The Software part consists of a Matlab/Simulink modeling tool that allows to program in real time the application concerned via specific blocks housed in the library "toolbox Real Time Interface (RTI)". In addition, the RTI can configure graphically the inputs/outputs.

Moreover, second software "ControlDesk" ensures the loading of the source program compiled and transformed into C code on the DS1104 R&D card. A second alternative of the ControlDesk software lies in the graphical interfaces creation for real-time controls and the recording of programs under files understandable by Matlab/Simulink or the evolution monitoring of the measured and calculated data in real time as illustrated in Fig. 13.

Prototyping GUIs essentially involves the following steps:

1. Using the Simulink modeling tool to build the control system.
2. The system simulation to generate the different control results.
3. Downloading the program in C code in dSPACE using the Real-Time Workshop (RTW) tool.
4. Real-time execution of the overall model while using the DS1104 R&D card.

The DS1104 R&D Controller Board is equipped the MPC8240 main Processor and the clock frequency of 250 MHz.

The connection of the dSPACE board with the WECS based on the Permanent Magnet Synchronous Generator is shown schematically in Fig. 14. As part of the Backstepping control experimental validation, tests were done using the dSPACE card and the Real-Time Workshop tool. Figs. 15 and 16 summarize the different results found for two tests. The first test is used to show the

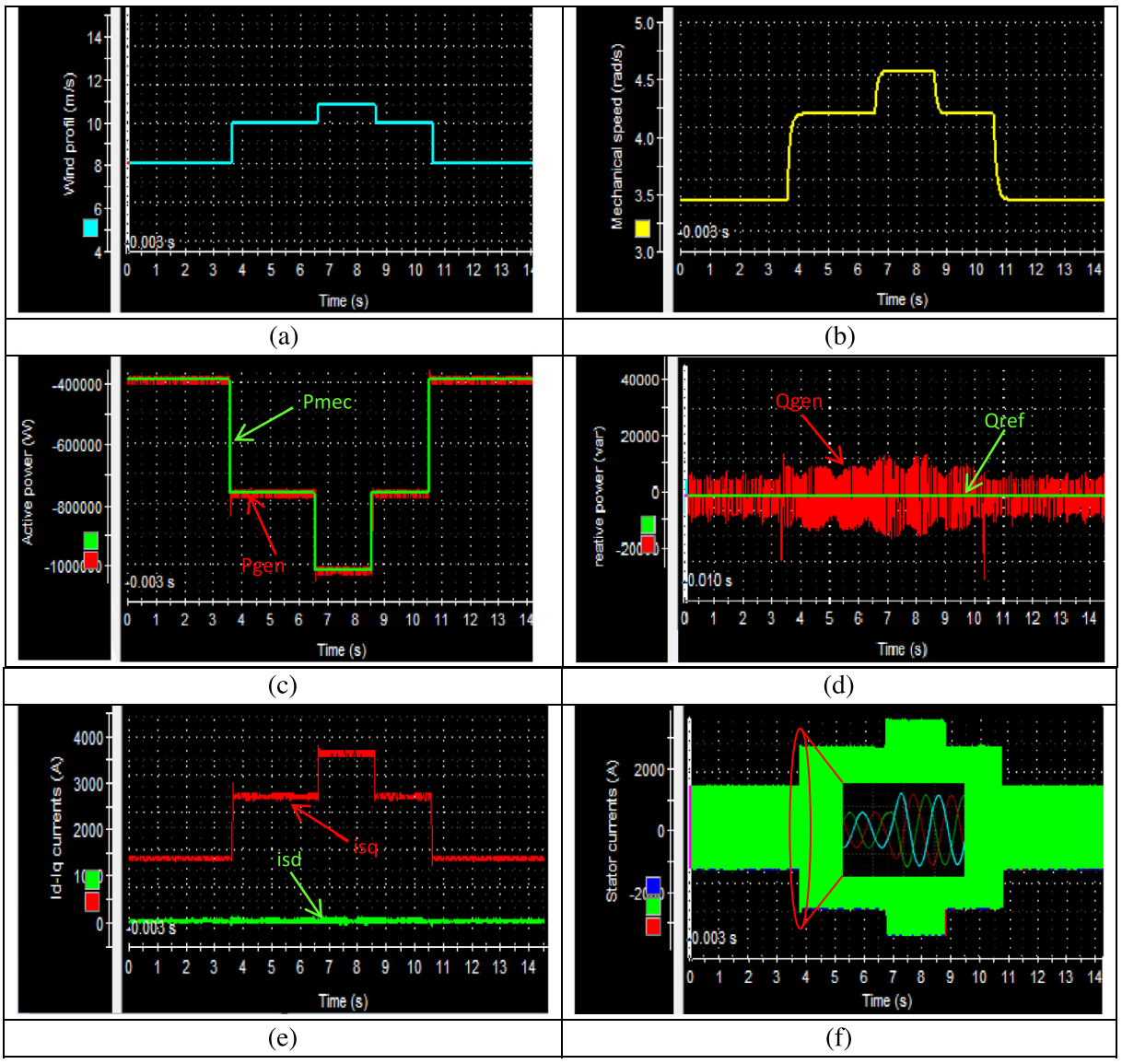

Fig. 15. Wind speed step figures: (a) Wind profile, (b) Mechanical speed, (c) Active power, (d) Reactive power, (e) direct and quadrature current, (f) stator current.

Table 3
The key features of the Backstepping control applied to WECS.

Measures	Ideal wind profile	Fluctuating wind profile
Power factor	0.999	0.999
Average mechanical powerPmec (W)	−7.4797e+005	−4.9675e+005
Average generator powerPgen (W)	−7.4796e+005	−4.9672e+005
Power efficiency(Pgen/Pmec) en %	99.99	99.99
Error power (W)	10	30
Power error rate in %	0.0013	0.0060
Response time (Pgen) in (ms)	8	–
Overshot (Pgen) in %	3	–

system robustness against a wind level profile, while the second proves the tracking efficiency and regulation following a fluctuating wind profile.

Figs. 15(c) and 16(c) clearly show the active power tracking with its mechanical reference. The finding is based on the generator power quality with a low ripple rate. The speed pursuit is clearly displayed in the power figures, not forgetting to mention the low overshoot in the abrupt change in reference power as shown in Fig. 15(c) successively at $t = 3.68$ s, $t = 6.6$ s , $t = 8.6$ s and at $t = 10.6$ s for example. Figs. 15(d) and 16(d) illustrate the reactive power forms with its reference $Q^*_{gen} = 0$ var. It is clearly remarkable that the reactive powers values in the two tests are reasonably low in comparison with the total power generated. A

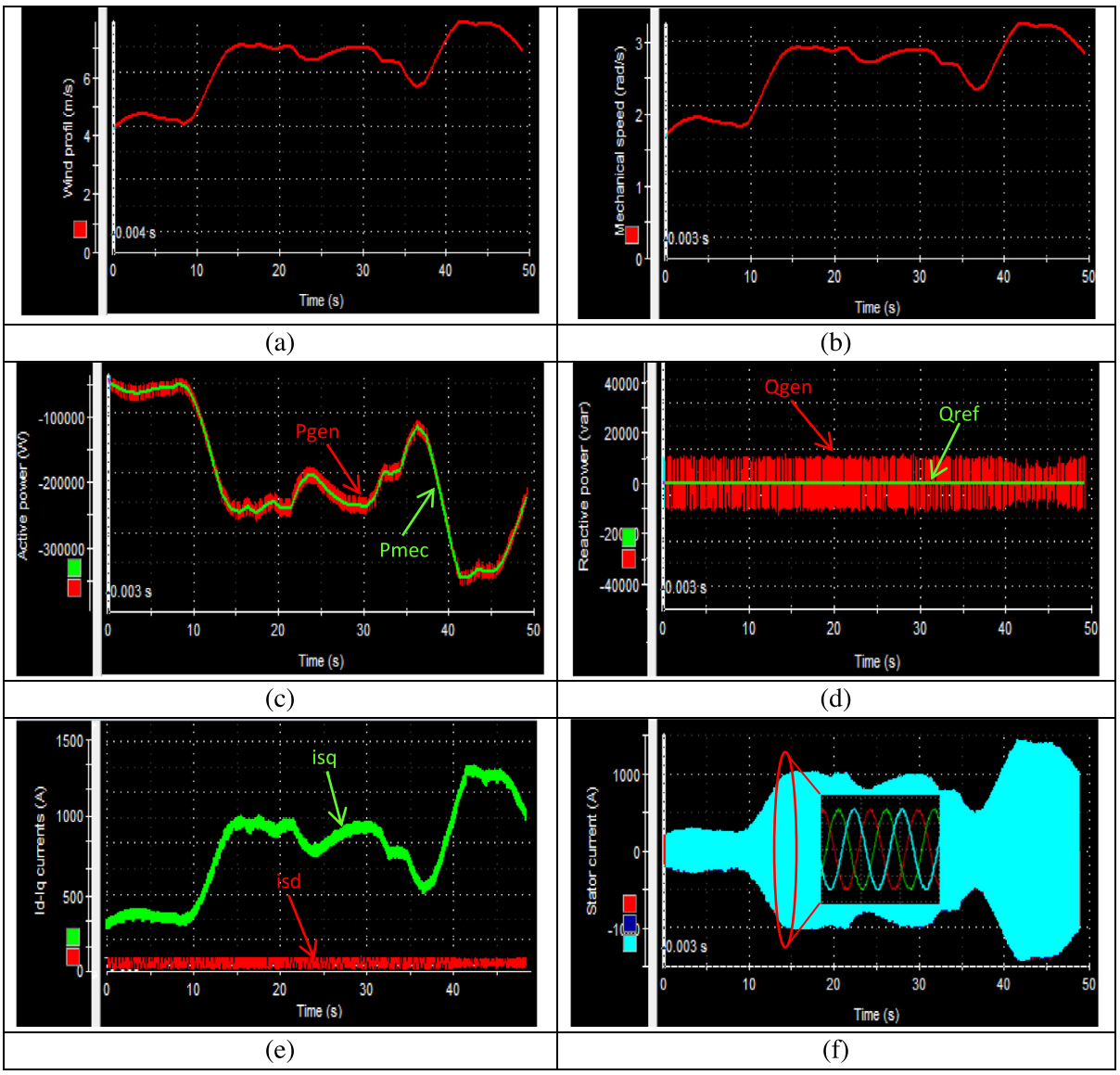

Fig. 16. Fluctuating wind speed figures: (a) Wind profile, (b) Mechanical speed, (c) Active power, (d) Reactive power, (e) direct and quadrature current, (f) stator current.

value that does not exceed 10 Kvar offers a power factor close to unity.

The mechanical angular speed curves follow perfectly the tracks traced for the wind profiles in the tests. Figs. 15(a) and 16(a) illustrate the wind profiles. Figs. 15(b) and 16(b) show the mechanical rotational speed tracking of the profiles plotted for the wind. It should be noted that the nonlinear Backstepping control offers better results both for the angular speed pursuit and for the powers generated.

The three-phase currents behavior in the various tests is illustrated in Figs. 15(f) and 16(f); similarly, the direct and quadrature stator currents are illustrated in Figs. 15(e) and 16(e). The wave forms as well as the pursuit rapid response are revealed according to the tests curves. It can be observed that the results obtained by experimentation are similar to those found in the simulation part either at the speed level or at the electric currents wave quality.

The nonlinear Backstepping control provides excellent results in this study. The reduced response time, the pursuit of the reference values and the regulation are the robustness terms which generally prove the efficiency obtained thanks to this control algorithm. Moreover, the practical results obtained make it possible to put a validation of the Backstepping control at the level of the WECS monitoring.

In order to validate the Backstepping control a table is put to compare the results found with some recently published works.

Table 4 is used to compare some results that generally attest to the proposed order quality. It should be mentioned that they do not refer to the same conditions since it is very difficult to find several works done under the same conditions. The work discussed in this article is based on the Backstepping control of a PMSG. The results achieved certify the high performance in the face of changes in the external elements and in the fixed setpoints pursuit. The proposed solution has a faster response and a better power factor than that obtained with the (FOPI) and (FFOPI + I) control of a PMSG in Beddar et al. (2016). Another comparison with an Asynchronous machine of (5.5 KW) in Abdelli et al. (2013) shows the quality proven by the proposed control in terms of power factor and energy efficiency.

Table 4
Performance comparison.

Publication paper	Technic methods	Generator	Overshot (%)	Efficiency (%)	Power factor	Performance
Abdelli et al. (2013)	FOC method Field oriented control (FOC)	IG (5.5 KW)	–	92.07	0.9997	Moderate-high
Abdelli et al. (2013)	Classical DTC method direct torque control (DTC)	IG (5.5 KW)	–	92.13	0.9711	Low
Abdelli et al. (2013)	MHDTC method Modulated hysteresis direct torque control (MHDTC)	IG (5.5 KW)	–	92.82	0.9993	Low
Beddar et al. (2016)	Fuzzy Order PI (FOPI)	PMSG	12	–	0.974	Moderate-high
Beddar et al. (2016)	Fuzzy Fractional Order PI+I (FFOPI+I)	PMSG	4	–	0.994	Moderate-high
Proposal technique	Backstepping method	PMSG (1.5 MW)	3	99.99	0.999	High

Table 5
The PMSG and wind turbine parameters.

Generator			Wind turbine		
Parameters	Symbol	Values	Parameters	Symbol	Values
Power Generator	P_n	1.5 MW	Radius of the turbine blade	R	40 m
pole number	P	35	Turbine and generator moment	J	1000 N·m
Stator Resistance	R_s	6.25e−3 Ω	Specific density of air	ρ	1.22 kg/m3
d axis inductance	L_d	4.229e−3 H	Tip-speed ratio	λ_{opt}	8
q axis inductance	L_q	4.229e−3 H			
Generator flux	$\varnothing_f$	11.1464 Wb	Optimal power coefficient	Cp_{max}	0.44
Coefficient of friction	f_c	0 N·m·s/rad			

7. Conclusion

This paper deals with a nonlinear Backstepping control applied to a variable speed wind energy conversion system based on PMSG. We first put the nonlinear control concept based on the Lyapunov stability technique in order to operate the WECS in best performance. Admittedly, the speed, the regulation and the follow-up of the setpoints are ensured by this control algorithm. PMSG modeling, WECS and Backstepping control theory are developed in this paper. A simulation using the Matlab/Simulink tool and the control implementation in the DS1104 R&D Controller Board for experimental validation are presented and discussed. The important conclusions of this study are:

- The nonlinear Backstepping control provides better performance in different wind profile situations.
- Robustness against variations in the wind profile is well assured through this control algorithm.
- The speed and the pursuit of the different sizes are ensured with better performances.
- The high energy efficiency and the power factor around the unit attest to the proposed control efficiency
- The simulation results show that the Backstepping control strategy provides better static and dynamic performance of a wind energy conversion system.
- We can affirm and validate the nonlinear Backstepping control effectiveness based on the experimental results that remain reliable and similar to those found in the simulation.

The future work will address the study of the dynamic performance of a PMSG-based wind energy conversion system for a load changing.

Abbreviations

AST	Adaptive Super Twisting
CPU	Central Processing Unit
DFIG	Doubly-Fed Electric Machine
DSIG	Dual Stator Induction Generator
DSP	Digital signal processor
DTC	Direct Torque Control
FOC	Field Oriented Control
FOPI	Fuzzy Order PI
FPGA	Field-Programmable Gate Array
GSC	Grid Side Converter
MHDTC	Modulated Hysteresis Direct Torque Control
MPPT	Maximum Power Point Tracking
MSC	Machine Side Converter
PI	Proportional Integral
PMSG	Permanent Magnet Synchronous Generator
PWM	Pulse Width Modulation
RTI	Real-Time Interface
RTW	Real-Time Workshop
SMC	Sliding Mode Control
SOSMC	Second Order Sliding Mode Control
ST	Super Twisting
TSR	Tip Speed Ratio
TTL	Transistor-Transistor Logic
WECS	Wind Energy Conversion System

References

Abbasi, S.A., Abbasi, T., 2016. Impact of wind-energy generation on climate: A rising spectre. Renew. Sustain. Energy Rev. 59, 1591–1598.

Abdelli, R., Rekioua, D., Rekioua, T., Tounzi, A., 2013. Improved direct torque control of an induction generator used in a wind conversion system connected to the grid. ISA Trans. 52 (4), 525–538.

Ahmed, A., Uddin, G.S., Sohag, K., 2016. Biomass energy, technological progress and the environmental Kuznets curve: Evidence from selected European countries. Biomass Bioenergy 90, 202–208.
Alemany, J.M., Arendarski, B., Lombardi, P., Komarnicki, P., 2018. Accentuating the renewable energy exploitation: Evaluation of flexibility options. Int. J. Electr. Power Energy Syst. 102, 131–151.
Anon., 2018, dspace digital signal processing and control engineering. https://www.dspace.com/fr/fra/home/products/hw/singbord/ds1104.cfm.
Beddar, A., Bouzekri, H., Babes, B., Afghoul, H., 2016. Experimental enhancement of fuzzy fractional order PI + I controller of grid connected variable speed wind energy conversion system. Energy Convers. Manage. 123, 569–580.
Bektache, A., Boukhezzar, B., 2018. Nonlinear predictive control of a DFIG-based wind turbine for power capture optimization. Int. J. Electr. Power Energy Syst. 101, 92–102.
Benakcha, M., Benalia, L., Ammar, A., Bourek, A., 2018. Wind energy conversion system based on dual stator induction generator controlled by nonlinear backstepping and pi controllers. Int. J. Syst. Assur. Eng. Manag. 1–11.
Benbouzid, M., Beltran, B., Amirat, Y., Yao, G., Han, J., Mangel, H., 2014. Second-order sliding mode control for DFIG-based wind turbines fault ride-through capability enhancement. ISA Trans. 53 (3), 827–833.
Bossoufi, B., Karim, M., Lagrioui, A., 2014a. MATLAB & Simulink simulation with FPGA Based Implementation adaptative and not adaptative backstepping nonlinear control of a permanent magnet synchronous machine drive. WSEAS Trans. Syst. Control 9, 86–100.
Bossoufi, B., Karim, M., Lagrioui, A., Taoussi, M., Derouich, A., 2015. Observer backstepping control of DFIG-generators for wind turbines variable-speed: FPGA-based implementation. Renew. Energy 81, 903–917.
Bossoufi, B., Karim, M., Lagrioui, A., Taoussi, M., El Hafyani, M.L., 2014b. Backstepping control of DFIG generators for wide-range variable-speed wind turbines. Int. J. Autom. Control 8 (2), 122–140.
Chen, Z., Guerrero, J.M., Blaabjerg, F., 2009. A review of the state of the art of power electronics for wind turbines. IEEE Trans. Power Electron. 24 (8), 1859–1875.
Cheng, M., Zhu, Y., 2014. The state of the art of wind energy conversion systems and technologies: A review. Energy Convers. Manage. 88, 332–347.
Djoudi, A., Bacha, S., Iman-Eini, H., Rekioua, T., 2018. Sliding mode control of DFIG powers in the case of unknown flux and rotor currents with reduced switching frequency. Int. J. Electr. Power Energy Syst. 96, 347–356.
Dogan, E., Seker, F., 2016. The influence of real output, renewable and non-renewable energy, trade and financial development on carbon emissions in the top renewable energy countries. Renew. Sustain. Energy Rev. 60, 1074–1085.
Domínguez-Navarro, J.A., Dufo-López, R., Yusta-Loyo, J.M., Artal-Sevil, J.S., Bernal-Agustín, J.L., 2019. Design of an electric vehicle fast-charging station with integration of renewable energy and storage systems. Int. J. Electr. Power Energy Syst. 105, 46–58.
Dragomir, G., Şerban, A., Năstase, G., Brezeanu, A.I., 2016. Wind energy in Romania: A review from 2009 to 2016. Renew. Sustain. Energy Rev. 64, 129–143.
El Mourabit, Y., Derouich, A., El Ghzizal, A., El Ouanjli, N., Zamzoum, O., 2017. DTC-SVM control for permanent magnet synchronous generator based variable speed wind turbine. Int. J. Power Electron. Drive Syst. 8 (4), 1732.
El Ouanjli, N., Motahhir, S., Derouich, A., El Ghzizal, A., Chebabhi, A., Taoussi, M., 2019. Improved DTC strategy of doubly fed induction motor using fuzzy logic controller. Energy Rep. 5, 271–279.
Errami, Y., Ouassaid, M., Maaroufi, M., 2015. A performance comparison of a nonlinear and a linear control for grid connected PMSG wind energy conversion system. Int. J. Electr. Power Energy Syst. 68, 180–194.
Fallahzadeh-Abarghouei, H., Hasanvand, S., Nikoobakht, A., Doostizadeh, M., 2018. Decentralized and hierarchical voltage management of renewable energy resources in distribution smart grid. Int. J. Electr. Power Energy Syst. 100, 117–128.
Fantino, R., Solsona, J., Busada, C., 2016. Nonlinear observer-based control for PMSG wind turbine. Energy 113, 248–257.
Global Wind Energy Council (GWEC), 2017. Global Wind Statistics 2016. https://www.statista.com/statistics/268363%20/installed-wind-power-capacity-worldwide/.
Hong, C.M., Chen, C.H., Tu, C.S., 2013. Maximum power point tracking-based control algorithm for PMSG wind generation system without mechanical sensors. Energy Convers. Manage. 69, 58–67.
Huang, S., Zhou, B., Li, C., Wu, Q., Xia, S., Wang, H., Yang, H., 2018. Fractional-order modeling and sliding mode control of energy-saving and emission-reduction dynamic evolution system. Int. J. Electr. Power Energy Syst. 100, 400–410.
Ionita, S., 2012. Regular paper nonlinear non adaptive backstepping with sliding-mode torque control approach for PMSM motor. J. Electr. Syst. 8 (2), 236–248.
Islam, M.R., Mekhilef, S., Saidur, R., 2013. Progress and recent trends of wind energy technology. Renew. Sustain. Energy Rev. 21, 456–468.
Kanellakopoulos, I., Kokotovic, P.V., Morse, A.S., 1991. Systematic design of adaptive controllers for feedback linearizable systems. In: 1991 American Control Conference. IEEE, pp. 649–654.
Kannan, N., Vakeesan, D., 2016. Solar energy for future world: A review. Renew. Sustain. Energy Rev. 62, 1092–1105.
Kortabarria, I., Andreu, J., de Alegría, I.M., Jiménez, J., Gárate, J.I., Robles, E., 2014. A novel adaptative maximum power point tracking algorithm for small wind turbines. Renew. Energy 63, 785–796.
Liu, Y., Wang, Z., Xiong, L., Wang, J., Jiang, X., Bai, G., et al., 2018. DFIG wind turbine sliding mode control with exponential reaching law under variable wind speed. Int. J. Electr. Power Energy Syst. 96, 253–260.
Lund, J.W., Boyd, T.L., 2016. Direct utilization of geothermal energy 2015 worldwide review. Geothermics 60, 66–93.
Mahela, O.P., Shaik, A.G., 2016. Comprehensive overview of grid interfaced wind energy generation systems. Renew. Sustain. Energy Rev. 57, 260–281.
Matraji, I., Al-Durra, A., Errouissi, R., 2018. Design and experimental validation of enhanced adaptive second-order SMC for PMSG-based wind energy conversion system. Int. J. Electr. Power Energy Syst. 103, 21–30.
Mérida, J., Aguilar, L.T., Dávila, J., 2014. Analysis and synthesis of sliding mode control for large scale variable speed wind turbine for power optimization. Renew. Energy 71, 715–728.
Nemmour, A.L., Mehazzem, F., Khezzar, A., Hacil, M., Louze, L., Abdessemed, R., 2010. Advanced backstepping controller for induction generator using multi-scalar machine model for wind power purposes. Renew. Energy 35 (10), 2375–2380.
Pacesila, M., Burcea, S.G., Colesca, S.E., 2016. Analysis of renewable energies in European Union. Renew. Sustain. Energy Rev. 56, 156–170.
Pareta, N., Sen, N., 2014. Modelling and simulation of permanent magnet synchronous motoer based wind energy conversion system. Int. J. Emerg. Res. Manag. Technol. 3, 43–52.
Prasad, S., Purwar, S., Kishor, N., 2019. Non-linear sliding mode control for frequency regulation with variable-speed wind turbine systems. Int. J. Electr. Power Energy Syst. 107, 19–33.
Rezaei, M.M., 2018. A nonlinear maximum power point tracking technique for DFIG-based wind energy conversion systems. Eng. Sci. Technol. Int. J. 21 (5), 901–908.
Shotorbani, A.M., Mohammadi-Ivatloo, B., Wang, L., Marzband, M., Sabahi, M., 2019. Application of finite-time control Lyapunov function in low-power PMSG wind energy conversion systems for sensorless MPPT. Int. J. Electr. Power Energy Syst. 106, 169–182.
Sun, T., Chen, Z., Blaabjerg, F., 2003. Voltage recovery of grid-connected wind turbines after a short-circuit fault. In: IECON'03. 29th Annual Conference of the IEEE Industrial Electronics Society, vol. 3, IEEE, pp. 2723–2728, IEEE Cat. No. 03CH37468.
Taoussi, M., Karim, M., Bossoufi, B., Hmmoumi, D., Lagrioui, A., Derouich, A., 2016. Speed variable adaptive backstepping control of the double-fed induction machine drive. Int. J. Autom. Control 10, 12–33.
Tummala, A., Velamati, R.K., Sinha, D.K., Indraja, V., Krishna, V.H., 2016. A review on small scale wind turbines. Renew. Sustain. Energy Rev. 56, 1351–1371.
Xiong, L., Li, P., Wu, F., Ma, M., Khan, M.W., Wang, J., 2019. A coordinated high-order sliding mode control of DFIG wind turbine for power optimization and grid synchronization. Int. J. Electr. Power Energy Syst. 105, 679–689.
Yang, B., Jiang, L., Wang, L., Yao, W., Wu, Q.H., 2016. Nonlinear maximum power point tracking control and modal analysis of DFIG based wind turbine. Int. J. Electr. Power Energy Syst. 74, 429–436.
Zamzoum, O., El Mourabit, Y., Errouha, M., Derouich, A., El Ghzizal, A., 2019. Active and reactive power control of wind turbine based on doubly fed induction generator using adaptive sliding mode approach. Int. J. Adv. Comput. Sci. Appl. 10, 397–406.
Zhang, H.B., Fletcher, J., Greeves, N., Finney, S.J., Williams, B.W., 2011. One-power-point operation for variable speed wind/tidal stream turbines with synchronous generators. IET Renew. Power Gener. 5 (1), 99–108.